Pergamon

Journal of Structural Geology, Vol. 17, No. 6, pp. 887 to 905, 1995
Elsevier Science Ltd
Printed in Great Britain

0191-8141(94)00099-9

An experimental study of the relationship between joint spacing and layer thickness

HAIQING WU and DAVID D. POLLARD

Department of Geological and Environmental Sciences, Stanford University, Stanford, CA 94305-2115, U.S.A.

(*Received* 8 *February* 1994; *accepted in revised form* 2 *September* 1994)

Abstract—Two methods for measuring joint spacing are described and compared. The *area method* is a constant for a given outcrop area and is not affected by joint distribution within that area; in contrast, the *line method* depends on the location of the linear traverse. Two kinds of joint sets are distinguished on bedding surfaces: (1) a *poorly-developed* set represents the early stages of development when typical joint lengths are less than typical spacing; (2) a *well-developed* set represents later stages when lengths are much greater than spacing. The area method is applicable to both poorly- and well-developed sets, whereas the line method produces inconsistent results for poorly-developed joint sets. Surface textures on many joints indicate point fracture origins and propagation parallel to bedding, whereas most numerical model studies of spacing assume linear origins and propagation perpendicular to bedding. The laboratory experiments described in this paper do not suffer from these restrictions. An important concept, confirmed during these experiments, is *fracture saturation*. When the applied strain reaches a certain value, fracture spacing stops evolving and remains nearly constant: these fracture sets are well-developed. Spacing at saturation is a function of layer thickness but is independent of strain, whereas spacing before saturation varies strongly with applied strain. Thus, plotting spacing vs thickness and comparing the slopes of lines fit to such data for poorly-developed joint sets in different layers is unlikely to be a diagnostic test for differences in material properties. On the other hand, spacing may be a sensitive indicator of strain for layers with poorly-developed joint sets. Assessing fracture saturation is a first-order consideration when gathering spacing data.

INTRODUCTION

FIELD observations for many, but certainly not all structural settings and lithologies indicate that joint spacing increases in some systematic fashion with the thickness of sedimentary strata (Narr & Lerche 1984). Quantitative data on this relationship are easily obtained from outcrop mapping, and such data may provide important constraints on the mechanical process of jointing. Having understood this process one is in a position to interpret the contribution of jointing to the geologic history of a particular rock mass. Thus, a first-order question for structural geologists working on the Earth's history is: what can one infer about the jointing process from field data on bed thickness and joint spacing?

Knowledge of the jointing process can also contribute to the solution of a number of very practical problems. For example, the development of accurate models for the flow of water (Barton & Larsen 1985, Deloule & Turcotte 1989, Cacas *et al.* 1990, Bear *et al.* 1993) and hydrocarbons (Nelson 1985, Thunvik & Braester 1990, Lorenz *et al.* 1991, Narr 1991) may depend on one's ability to predict the spacing of joints at depth in aquifers and reservoirs. Unlike the abundant data available from outcrops, the opportunities to obtain joint spacing data in the subsurface are usually limited to observations made in wells. Thus, an important challenge for structural geologists working on fractured aquifers and reservoirs is: how can one extrapolate the data on joint spacing obtained from boreholes into the surrounding sedimentary formations? We suggest that such extrapolations should be based on an understanding of the physical process of jointing.

In this paper, the term 'joint' refers to those natural fractures with field evidence for dominantly opening displacement (Pollard & Aydin 1988) and the term 'fracture' refers to those with opening displacement, but produced in experiments using model materials. The term 'spacing' means the perpendicular distance between two neighboring, parallel joints or fractures.

Joint spacing in outcrops

The structural literature contains many examples of outcrop data sets on the relationship between joint spacing and bed thickness from linear (Figs. 1a–c) to non-linear (Figs. 1d & e) with increasing range of thickness. For example, Price (1966) reported that Bogdanov (1947), Novikova (1947) and Kirillova (1949) found approximately linear relationships between mean joint spacing, D, and bed thickness, T, for two sandstones, and a limestone from Russia (Fig. 1c). Treating spacing as the dependent variable and thickness as the independent variable, one can fit a straight line to each data set such that $D = \alpha_i T$. From these data one could conclude that the slopes, α_i, of these lines do not change with thickness, but are a function of lithology and, by inference, of mechanical properties. Various later papers (Lachenbruch 1961, Hobbs 1967, Sowers 1973, Price & Cosgrove 1990, Narr 1991, Narr & Suppe 1991, Gross 1993) also suggest a linear relationship between joint spacing and bed thickness.

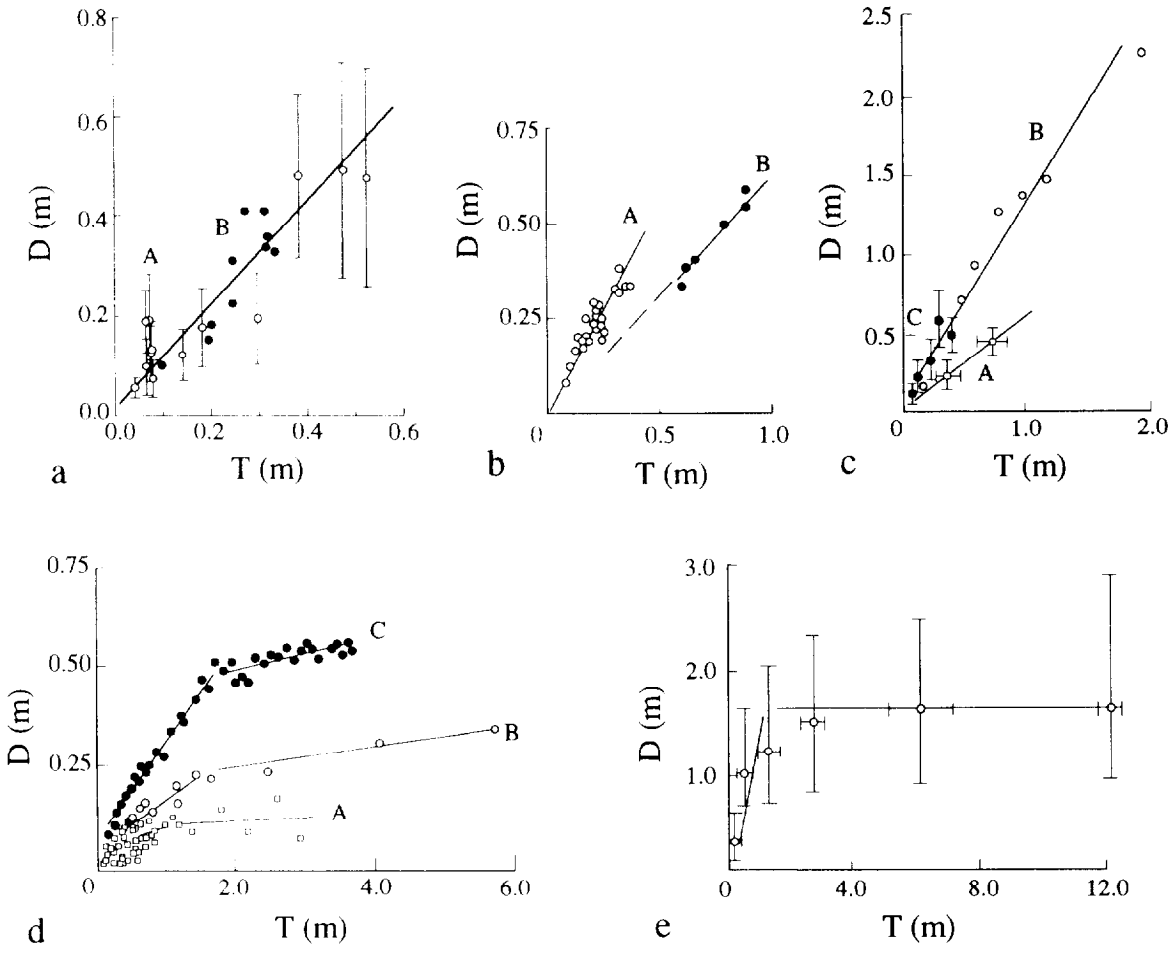

Fig. 1. The relationships between joint spacing, D, and bed thickness, T, presented by different authors. (a) Clayey–siliceous member of the Miocene Monterey Formation at Gaviota, California, U.S.A. A: data with error bars from the authors of this paper; B: data (solid dots) from Gross (1993). (b) Limestones from Bevons syncline, near Sisteron, southern France (after Huang & Angelier 1989). A: Albian limestones; B: Neocomian limestones. (c) Two different lithologies from Russia (Bogdanov 1947, Novikova 1947, Kirillova 1949, after Price 1966). A, B: sandstones; C: limestone. (d) A: Portuguese greywacke; B: U.K. greywacke; C: U.K. greywacke (after Ladeira & Price 1981). (e) Asmari limestone, Iran (after McQuillan 1973).

Huang & Angelier (1989) found that limestones from two different places on the Bevons syncline near Sisteron, southern France, have different but nearly constant values of α_i (Fig. 1b). From these data one could conclude that α_i is a function of structural position and, by inference, of deformation. Support for that conclusion comes from relatively hard reservoir rocks of the Monterey Formation which show a Fracture Spacing Index, FSI = $1/\alpha_i$, that varies from about 0.1 to 0.5 with structural position on a fold in the subsurface (Narr 1991). In contrast, Narr (1991) found much greater values of FSI in outcrops with thicknesses up to 2.5 m. Furthermore, all values of FSI for these surface exposures were practically the same, about 1.3, for different hard rock types and in different structural locations.

The linear relationship between bed thickness and joint spacing has been widely accepted as a general description, with a few exceptions (Norris 1966, Mastella 1972). However, many of the reported field observations were conducted in beds less than 1.5 m thick. In some cases, for layer thickness exceeding 2 or 3 m, the simple linear relationship is no longer appropriate. For example McQuillan (1973) and Ladeira & Price (1981) investigated joint spacing in layers up to 12 m thick and suggested a relationship based on two straight lines (Figs 1d & e). Cruikshank & Aydin (in press) observed that joint spacing is only about 0.3 times a bed thickness of 40 m, much smaller than spacings in thinner layers. Price & Cosgrove (1990) explained this bilinear relationship by proposing two different mechanisms: spacing in thin layers is influenced by tractions at the competent–incompetent rock interfaces, whereas spacing in thick layers is independent of bed thickness and results from an hydraulic fracture mechanism. On the other hand, a continuous curve with a positive slope and a negative second derivative also provides a reasonable fit to these data:

$$\frac{dD}{dT} > 0 \quad \text{and} \quad \frac{d^2D}{dT^2} < 0. \tag{1}$$

This avoids the discontinuity in slope and may obviate the need for two different physical mechanisms (Angelier *et al.* 1989, Soufaché & Angelier 1989).

Motivation for this research

Although joint spacing is found to be roughly proportional to layer thickness in many studies, these data

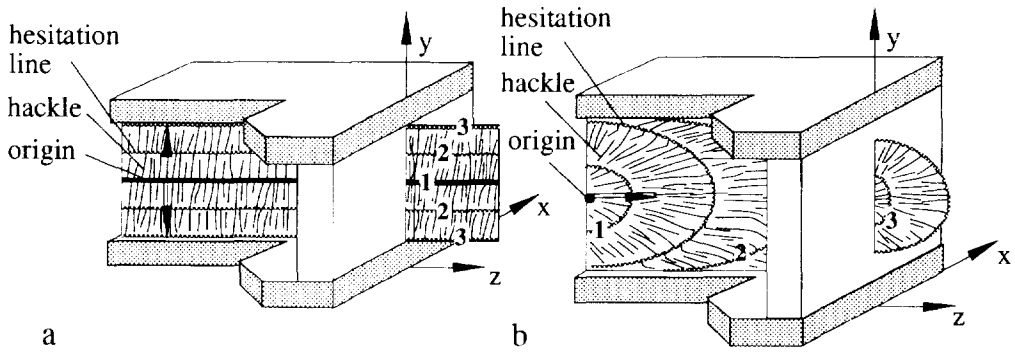

Fig. 2. Comparison of joint propagation direction and surface textures: (a) in an idealized two-dimensional model; and (b) in a more realistic three-dimensional model (modified after Hodgson 1961). Hackle trend in the propagation direction.

sets are not all consistent with one another and they have led to contradictory conclusions about the jointing process. One possible explanation is that the data collection methods have been inappropriate. In the most common field method, spacing is measured along a line (scanline) perpendicular to the average strike of the joint set, either on cross-sections of a layer or on the bedding surface of a layer. In this paper we describe possible shortcomings on the *line* method and suggest an alternate *area* method for measuring joint spacing on bedding surfaces, based on quantitative stereological practice (Underwood 1972).

A second possibility is that the physical relationship between spacing and thickness is inadequately understood. Indeed, the development of a joint set is a complex three-dimensional process with a variety of possible temporal changes in physical conditions and loading (Hancock 1985, Engelder 1987, Pollard & Aydin 1988). Direct evidence for a time sequence and for the complexity of three-dimensional spatial relations can be found by inspection of joint surface textures (Kulander *et al.* 1979, DeGraff & Aydin 1987, Bahat 1991). From a mechanical point of view it is reasonable to express some skepticism that such a process could produce a simple linear, or even bilinear relationship between spacing and thickness (Rives *et al.* 1992).

Most mechanical models that address the spacing–thickness relationship (e.g. Hobbs 1967, Pollard & Segall 1987, Narr & Suppe 1991, Zeller & Pollard 1992, Gross 1993, Gross *et al.* in press) take a two-dimensional view of joints in which they propagate in a plane perpendicular to bedding and perpendicular to the strike of the joint set (in the *xy*-plane of Fig. 2a). In the block diagrams of Fig. 2 rib marks (hesitation lines) are indicative of a temporary fracture front and hackle are aligned in the local propagation direction (Helgeson & Aydin 1991). If propagation of joints were confined to the *xy*-plane, the origin and the rib marks would be horizontal lines and the hackle would be vertical lines (Fig. 2a). This pattern of surface textures is not observed on joints. Although each of the models mentioned above has contributed to progress in the mechanical analysis of joint spacing, an obvious problem is that they ignore the temporal and three-dimensional evolution of a joint set.

Typical patterns of surface textures on joints in sedimentary rocks (Woodworth 1896, Hodgson 1961, Price 1966, Syme-Gash 1971) include an origin at a point, rib marks that are convex in the propagation direction, and hackle that spread out in a fan-shaped pattern (Fig. 2b). Fracture propagation near the origin is radial, but after the fracture terminates at the top and bottom surfaces of the jointed layer, the dominate propagation directions are sub-parallel to the bedding plane. For example, field observations of joint surface textures at Davenport, California, provide compelling evidence for the lateral propagation of joints. Figure 3 is typical: subhorizontal hackle indicate a dominantly horizontal propagation direction. Rib marks extend as curving arcs from the top to the bottom of the layer and their convexity indicates propagation from left to right. The fracture origin in this case is out of the field of view to the left. Not only should models of the jointing process in sedimentary sequences include lateral propagation, the common occurrence of this phenomenon raises doubts about the usefulness of field data taken along scan lines on cross-sections of a layer (on the *xy*-plane of Fig. 2a).

We have investigated experimental models that share many of the kinematic features, such as lateral propagation, with the fracture idealized in Fig. 2(b) and, presumably, with the joint illustrated in Fig. 3. In this paper we describe a series of experiments, using a brittle coating technique (Garrett & Bailey 1977a,b, Pollard *et al.* 1990, Rives & Petit 1990a, Wu & Pollard 1991, 1992a,b) in which the evolution of a fracture set is monitored during a controlled loading sequence, thus providing direct observations of the different stages in the development of the set (Fig. 4). By changing the thickness of the brittle coating we are able to examine how spacing is dependent upon thickness at each stage of development.

Rives *et al.* (1992) have studied how the frequency distribution of spacing, as measured using the line method, depends on the stage of development of fracture sets. They characterize three stages with three different frequency distributions (negative exponential, log–normal, and normal) for the spacing of fractures in polystyrene plates subject to pure bending and suggest that the ratio of mode to mean for such distributions is a good indicator of how well developed the set is. By analogy, Rives *et al.* (1992) used the mode-to-mean ratio

of these frequency distributions to identify the stage of development for joint sets from three localities in the United Kingdom. We follow a similar line of reasoning in this paper, but emphasize how knowledge of the developmental stages of a joint set can be brought to bear on interpretations of the relationship between joint spacing and layer thickness.

Our experimental models also highlight the desirability of observing joint sets on bedding planes. Because propagation is dominantly parallel to bedding, such exposures reveal aspects of the geometry and spatial distribution of joints that are not visible in layer cross-sections. This suggests that measures of spacing should take advantage of the aerial distribution of joints as exposed on bedding planes wherever possible. In the next section we describe such a measurement technique and then return to a detailed discussion of the experimental models.

MEASUREMENT OF SPACING FOR WELL- AND POORLY-DEVELOPED JOINT SETS

To study the geometry of fracture sets at different stages of development we need a consistent method to measure spacing. Qualitatively, we observe two end-members in the series of fracture patterns developed in a particular laboratory specimen (Fig. 5). One is termed *poorly-developed* because it is characteristic of the early stages of development in which typical fracture lengths are roughly equal to or less than typical spacings (Fig. 5a). The other one is termed *well-developed* because it is characteristic of the later stages in which fracture lengths typically are much greater than spacings (Fig. 5b). Not all methods of measuring spacing are effective for both of these geometries.

The common method for measuring fracture spacing is a *line* (or *scanline*) *method* (Fig. 6a). Traverses are taken perpendicular to the average strike of the set either along cross-sections of a layer or along the surface of a layer to estimate the quantity D, defined as:

$$D = \frac{l}{n+1} \quad \text{or} \quad D = \frac{1}{n+1}\sum_{i=0}^{n} D_i. \tag{2}$$

Here D_i is the perpendicular distance between two neighboring joints and n is the number of joints between the two end-points of the traverse, which are separated by a distance l and are not at fractures. Although this method provides consistent measures of D for a well-developed fracture pattern (Fig. 5b), values for a poorly-developed pattern can be widely scattered and dependent on where the traverse is taken (Fig. 5a). For example, values of D for traverses taken at different positions, x, across the poorly-developed set in Fig. 5(a) vary from 3.2 mm to 6.7 mm. In contrast the range of values for the well-developed set in Fig. 5(b) varies only from 0.9 mm to 1.3 mm.

An *area method* for measuring the mean spacing, S, is suggested in this paper, based on quantitative stereological practice (Underwood 1972). This method does not apply to cross-sections of a fractured layer, rather it assumes that a surface of the layer is exposed. The area method defines spacing as:

$$S = \frac{A}{l_0 + \sum_{i=1}^{n} l_i} = \frac{A}{l_0 + L}, \tag{3}$$

where l_0 is the side length of a square measuring region, L is total length of fracture i in that region, n is the number of fractures in the square, and $A(= l_0^2)$ is the area of the square.

To distinguish the two measures of spacing we use S for the area method and D for the line method. The difference between them is that S is only a function of A and L, but D depends on traverse position (x). For a well-developed fracture pattern, most fractures cross the entire square so we have $l_i \approx l_0$. In this case (3) becomes

$$S \approx \frac{l_0^2}{(n+1)l_0} \approx D \qquad (l_i \to l_0)_0. \tag{4}$$

Thus the two methods produce the same result for this end-member of the stages of fracture development. In a more general form, useful for outcrop studies, the mean spacing can be expressed for a regular polygonal area (Fig. 6b) if fracture lengths and the coordinates of enough peripheral points are measured. This method is readily applied in the field using a total station or in the laboratory using a digitizer for mapped data. The details are provided in Appendix A.

Scale effect on the area method

Strictly speaking the precision of the area method depends on how precisely one can measure the area and the total fracture length. However, an important consideration is the size of the measurement area relative to a characteristic length scale for the fractures. If the area is too small the sample will not be representative of the fracture set; if the area is too big it may include real spatial variations in mean spacing. To design a measurement strategy one would like to know how large an area is proper for the area method.

Figure 7 illustrates how mean spacing, based on the area method, depends on the size of the measurement area for poorly- and well-developed fracture sets from our laboratory experiments. We take three small squares shown in the upper right corner of Fig. 7(a) and change their side length from 0.5 mm to 80 mm. The calculated spacings as a function of side length are plotted in Fig. 7(a) for the poorly-developed case and in Fig. 7(b) for the well-developed case.

The dotted curves in the lower part of each figure give the total error defined as:

$$E_{\text{area}} = \sqrt{\frac{1}{m_1}\sum_{i=1}^{m_1}\left(\frac{S_i}{S_0} - 1\right)^2}, \tag{5}$$

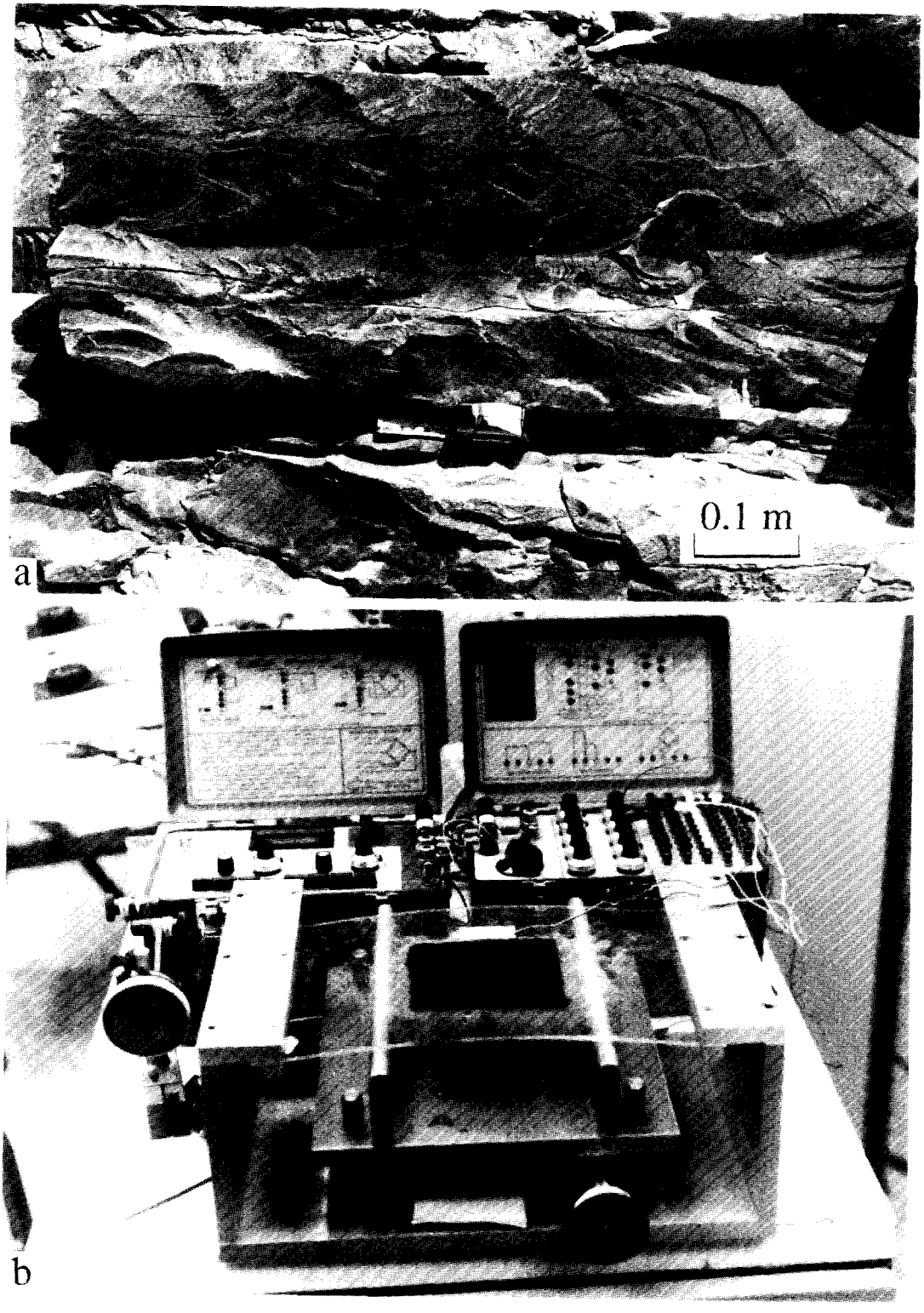

Fig. 3. (a) Textures on a joint surface shown in Davenport, California. The fracture origin of this joint is to the left of the photo. Hackle and hesitation lines indicate lateral propagation to the right. (b) A four point-bending device used to produce a fracture set in a brittle coating.

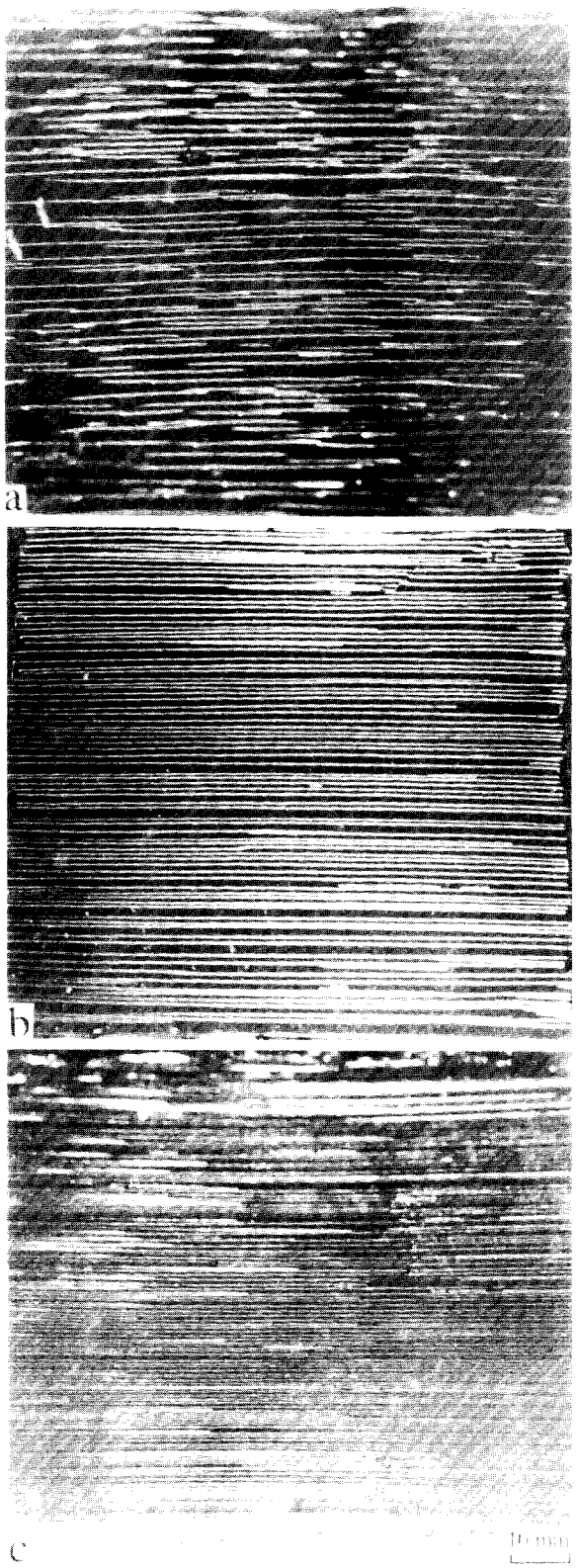

Fig. 4. Fracture patterns of typical experiments with different thicknesses, T, of brittle coating (#10 PMMA sheet). L is total length of fractures and S is spacing measured with the area method (all units: mm): (a) $T = 0.249$, $L = 3.4 \times 10^3$, $S = 2.86$; (b) $T = 0.189$, $L = 7.1 \times 10^3$, $S = 1.40$; (c) $T = 0.078$, $L = 1.7 \times 10^4$, $S = 0.58$.

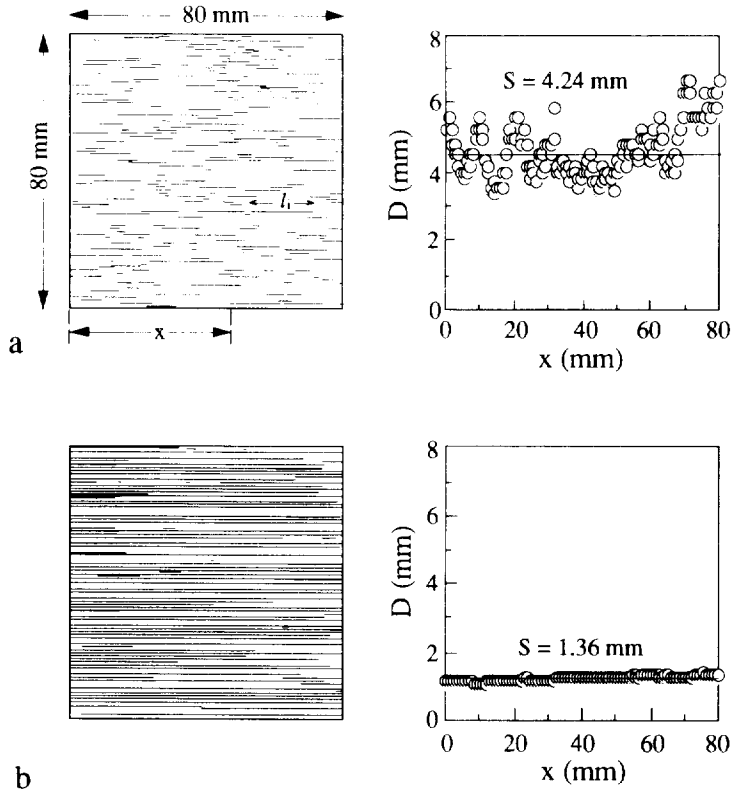

Fig. 5. Comparison of line spacing, D, and area spacing, S, for poorly- and well-developed laboratory fracture patterns. (a) A poorly-developed pattern with short fractures. The right graph is scattered readings of spacing, D, as a function of scanline position, x. Solid line represents the mean spacing, S, defined by area method. (b) A well-developed pattern where most fractures cross the sample square.

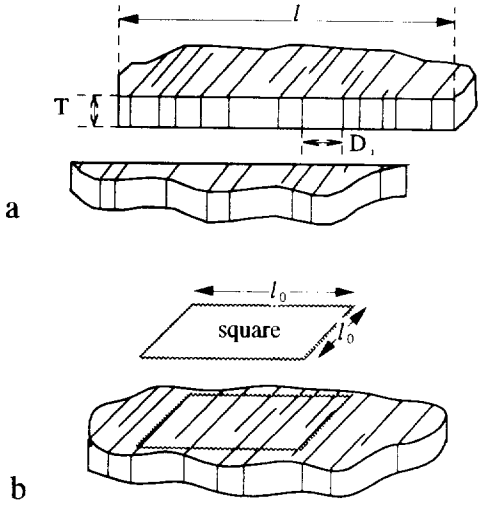

Fig. 6. Illustration of how spacing is measured in two ways for outcrops or laboratory samples. (a) For the line method the traverse distance, l, is divided by the number of joints crossed plus one. Spacing varies as traverses are positioned at different locations. (b) For the area method the total joint length, L is divided by the area of the counting square, $A = l_0^2$.

where m_1 is the number of small squares, S_0 is the spacing for the whole area (l_0 = 80 mm) and S_i is the spacing for the small square i. If $m_1 = 1$, the error becomes $E_{area} = |S_1 - S_0|/S_0$. For the poorly-developed fracture set in brittle coating shown in Fig. 5(a), the error is less than 10% when l_0 exceeds about 44 mm (dashed line in Fig. 7a). For the well-developed fracture set (Figs. 5b and 7b), the error is less than 10% when l_0 exceeds about 22 mm. Clearly these are not unique relationships for fracture sets in brittle coatings, but an error analysis such as this one can be used to justify the size of areas used for measurement.

Comparison of the line method and the area method

Experimental results using the two methods are compared on the right-hand graphs in Figs. 5(a) & (b). Spacings represented by the scattered data points are obtained by the line method defined in equation (2). Solid straight lines represent spacings obtained by the area method defined in equation (3). The comparison shows that the two methods produce very similar results for a well-developed fracture pattern. However, for a poorly-developed pattern, the line method produces scattered results that vary by more than 50% from the value of S.

A field example of a poorly-developed joint pattern is shown in Fig. 8(a) taken from a Carboniferous sandstone outcrop, located at a coastal exposure in southwestern Wales mapped by Dunne & North (1990). Spacings measured using the two methods are shown in Fig. 8(b). The polygonal area with 22 points along its periphery is about 189 m^2, and the total fracture length is about 100 m. The dimension l_0 in the x direction is 10 m. Thus the mean spacing S for the entire outcrop is about 1.7 m. Using the line method (2), the spacing D ranges from 2.5 m near the left edge to 1.0 m near the right edge of the outcrop and varies, depending on location x within the outcrop.

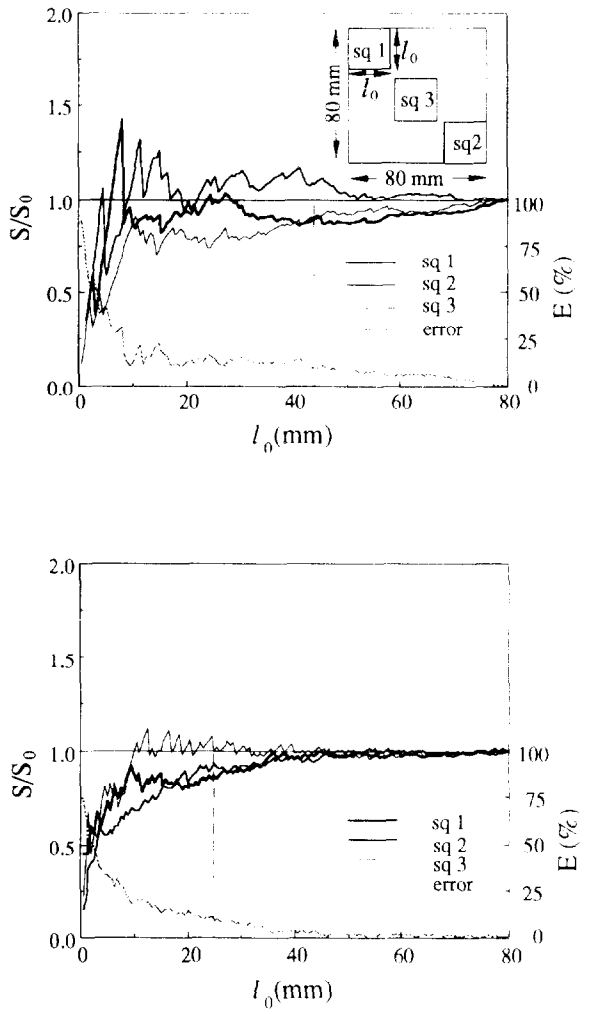

Fig. 7. Example of the scale effect on the area method. The curves of the normalized spacing for three squares with side length, l_0, changing from 0.5 to 80 mm are compared with the spacing for a 80 × 80 mm square, S_0. The dotted curves in the lower part of each graph are the errors for the area method. The vertical dashed lines indicate the minimum l_0 for an error of about 10%: (a) The *poorly-developed* case: S_0 = 4.24 mm, l_0(<10% error) = 44 mm (b) The *well-developed* case: S_0 = 1.36 mm, l_0(< 10% error) = 25 mm.

The error for the line method as compared to the area method is defined as:

$$E_{\text{line}} = \frac{D - S}{S}, \tag{6}$$

$$D = \frac{1}{m_2} \sum_{i=1}^{m_2} D_i, \tag{7}$$

where m_2 is the number of measurements using the line method, and D_i is the ith measurement. The corresponding errors calculated using (6) for individual traverses of the joint set shown in Fig. 8(a) vary from 0 to 53%. On the other hand, the area method provides a constant fracture spacing for this outcrop that is independent of traverse position for the line method.

The second example, Fig. 9(a) shows an outcrop of Entrada Sandstone on the southwest limb of Salt Valley anticline within the late Paleozoic Paradox formation at Arches National Park, Utah, mapped by Cruikshank & Aydin (in press). This outcrop displays a joint set in a well-developed state. The polygonal area with 14 points along its periphery is about 482,000 m^2, and the total fracture length is about 12,900 m. The dimension l_0 in the x direction is about 694 m. Spacings obtained using the line and area methods are compared in Fig. 9(b), where it can be seen that D ranges from 23 m to 40 m and S is 35.4 m. The values of D are less scattered about S than those for the *poorly-developed* joint set shown in Fig. 8.

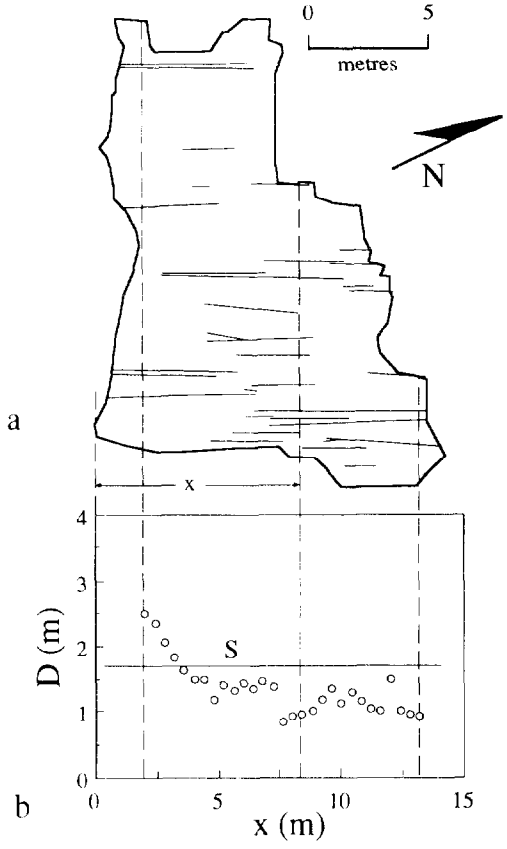

Fig. 8. Field example of a poorly-developed joint set. (a) Map of sandstone outcrop from southwestern Wales (after Dunne & North 1990). (b) Spacings, D and S, measured by the two methods: scattered data points for the line method and a solid line for the area method. A = 189 m^2, L = 100 m, l_0 = 10.0 m and S = 1.7 m.

Since the area method avoids personal choices on measurement location and direction, we conclude that the area method is superior to the line method and recommended that future measurements of fracture spacing, both in the laboratory and in the field, utilize this method if possible.

EXPERIMENTAL MODELING

Experimental design

The technique uses a brittle coating (methylene chloride) on a PMMA (polymethyl methacrylate) substrate (Pollard *et al.* 1990, Wu 1991, Wu & Pollard 1991, 1992a,b). This technique can provide valuable insight concerning fracture processes that are impossible to observe in nature and difficult to consider using numerical models. A similar technique has been developed by

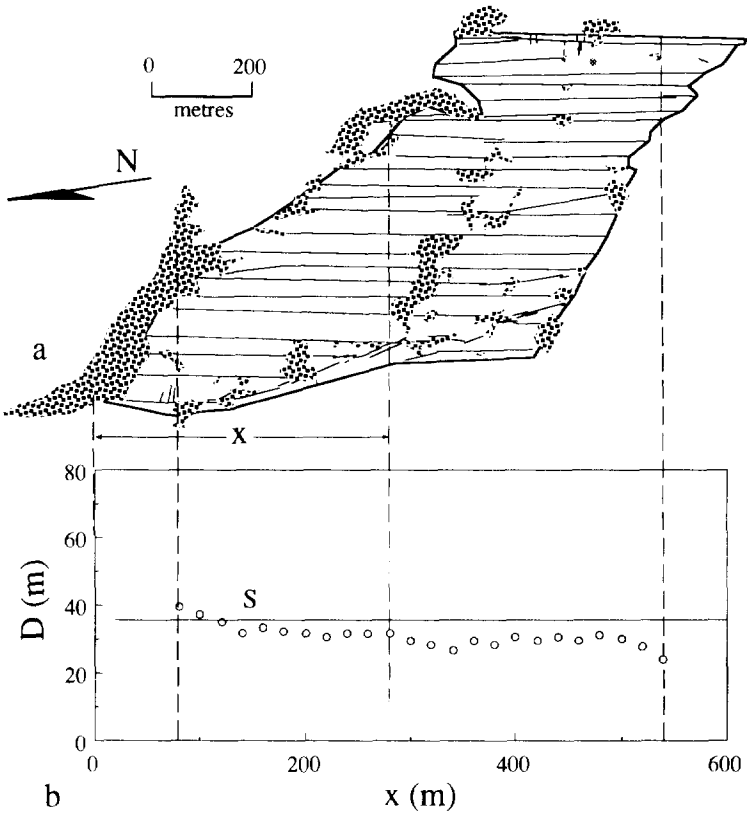

Fig. 9. Field example of a well-developed joint set from Arches National Park, Utah. (a) The fracture pattern mapped at a sandstone outcrop (after Cruikshank & Aydin in press). (b) Spacing measured by the two methods: scattered data points for the line method and a solid line for the area method. A = 482,000 m^2, L = 12,900 m, l_0 = 694 m, T = about 40 m and S = 35.4 m.

Rives & Petit (1990a,b), and Rives *et al.* (1992) using polystyrene substrate. The technical difficulty of initiating a fracture set for studying spacing in the laboratory comes about because of the instability of fracture propagation: typically only one fracture propagates under a certain stress value even though many pre-existing fractures are cut in an isolated sample. Unlike most other laboratory fracture experiments in which only one or a few fractures are developed (Rossmanith 1983, Mihashi *et al.* 1989), our technique can produce a set with up to a few hundred fractures without failure of the entire specimen. Furthermore, because of the stable propagation of fractures, we can document the time dependent behavior of this system.

The PMMA sample is about 0.45 cm thick and 20 × 30 cm in dimension, and the brittle coating covers a square of 10 × 10 cm. The fractures can be easily seen with appropriate oblique lighting (Wu & Pollard 1991), so data were taken from photographs and corrected for the oblique view of the camera. Fractures initiated at small bubbles and other unperfections in the coating. Fracture length is not a function of flaw size if the fracture is much longer than the flaw diameter (Rives *et al.* 1992). Because the typical diameter of bubbles in the coating is 10–30 μm, fractures only 1 mm in length have a ratio of length to flaw size as great as 30–100.

The different thicknesses of dried brittle coatings were 0.016, 0.031, 0.078, 0.125, 0.189, 0.249 and 0.373 mm corresponding to 0.5, 1, 2.5, 4, 6, 8 and 12 cc of fluid coating, respectively. Ten different pieces of PMMA sheet were used as the substrate. Figure 4 shows three typical experiments with thicknesses of 0.078, 0.189 and 0.249 mm using the same substrate. For each thickness from seven to 11 samples were tested under the same loading conditions and a total of 67 experiments were conducted.

A four point-bending device (Rives *et al.* 1992, Wu 1992) shown in Figs. 3(b) and 10 serves to impose a uniform extensional strain on the top boundary of the PMMA sheet and strain gages measure this longitudinal strain. The strain in the brittle coatings was calculated based upon conventional thin plate bending theory (Timoshenko & Woinowshy-Krieger 1959) and the assumption of perfect bonding between the two materials. Different coating thicknesses, T, were tested with the same total strain and the same loading conditions (Fig. 10). The applied maximum strain was $\varepsilon_0 = 4.5 \times 10^{-3}$ and a typical duration of loading was about 2 min.

Edge effect

A potential problem with our experimental design is the effect played by the edges of the brittle coating on fracture spacing. By 'edge effect' we mean the fact that the coating is not continuous, but is confined to a 100 mm by 100 mm square region, yet some fractures propagated all the way to the edges and some actually initiate at flaws along one or the other edge. Conceivably the spacing could be influenced by these edges so we would

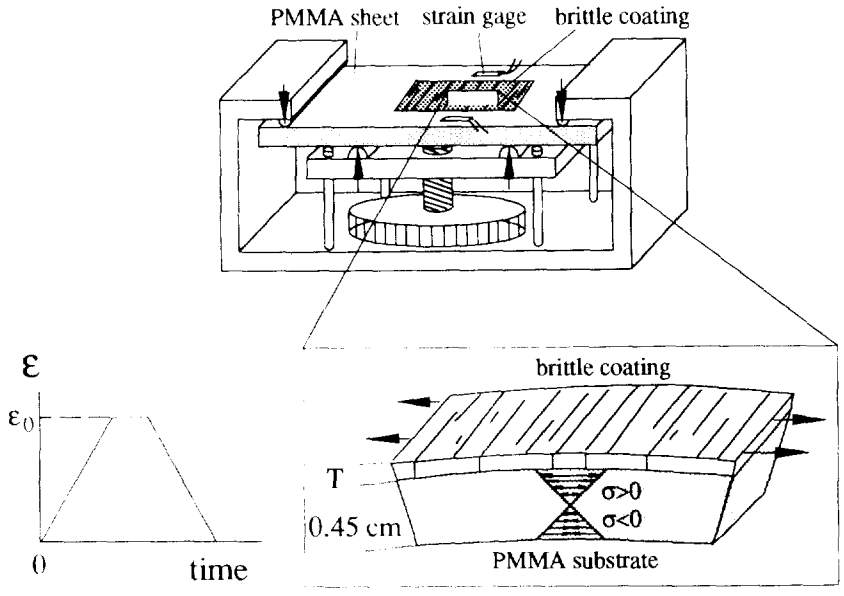

Fig. 10. A four-point bending device applies a pure extension on the top of a 20 × 30 cm PMMA sheet. A thin layer of brittle coating in a 10 × 10 cm square is bonded to the PMMA substrate which transmits a uniform strain to the coating. Layer thickness T of the brittle coating changes from 0.016 to 0.373 mm. Inset shows applied strain as a function of time. ε_0 is maximum strain.

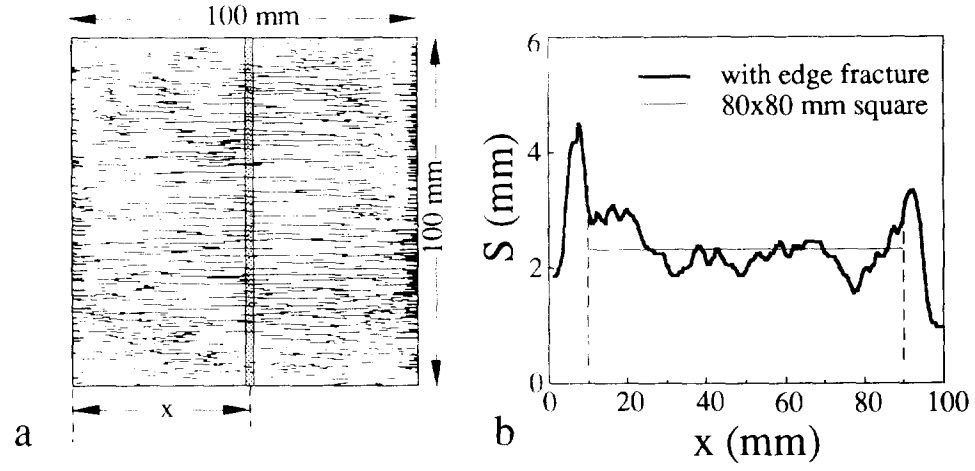

Fig. 11. Evaluation of the edge effect on spacing for a maximum applied strain of $\varepsilon_0 = 3.8 \times 10^{-3}$. (a) Map of fractures; those initiated from edges are marked by thicker lines. The area method is used to calculate fracture spacings. The measurement area is 2 × 100 mm as shown by the shaded rectangular and the distance from the origin to the center of the rectangular is x. (b) Spacing distribution as a function of position x. The thin line represents spacing in a 80 × 80 mm internal square.

not be able to produce spacing values representative of a continuous layer. In that case, we would have to use a larger sample to reduce or eliminate this effect.

During typical experiments many fractures initiated from the edges and propagated toward the center. However, most of these fractures terminated at lengths of 1–5 mm because they overlapped other fractures propagating from the edge or the interior. Indeed, many of the fractures which appear to extend from one edge to the other in the well-developed sets (Fig. 4) actually are composed of several closely-spaced echelon segments. None-the-less, we designed a method, described below to evaluate the edge effect on spacing.

Figure 11(a) shows a typical experiment with an applied strain of $\varepsilon_0 = 3.8 \times 10^{-3}$. Many short fractures initiated from the edges and are highlighted there by thicker lines. The area method is used to calculate fracture spacings in a narrow sampling window, 2 × 100 mm in size (the shaded rectangle in Fig. 11a). For measurement purposes x is the distance from the left-hand edge of the coating to the center of the sampling window. The spacing distribution as a function of x (Fig. 11b) demonstrates that some spurious results do occur when the sampling window is within about 10 mm of the edges. On the other hand, S for the 100 × 100 mm square is 2.27 mm and S for a centered 80 × 80 mm square is 2.31 mm. The thin straight line in Fig. 11(b) represents S for the 80 × 80 mm square. We conclude that the size of the coated area in our experiments was sufficient to avoid significant edge effects.

There is almost no edge effect if the fracture set is poorly developed since, at low applied strains, fractures initiate more easily inside the brittle coating than along the boundaries.

Fracture saturation

Scattered data points of mean spacing, S, vs applied strain, ε, for seven thicknesses are plotted in Figs. 12(a)–(g). The applied strains increased up to 5.5×10^{-3} in these experiments and 13–14 readings of spacing and applied strain were taken for each experiment. All of the experiments produced a similar relationship between spacing and thickness: spacing decreases rapidly with strain in the early stages of the experiment and then decreases less rapidly, finally reaching a nearly constant value. In other words, a greater applied strain beyond some limiting value will not change the spacing significantly (Wu 1991, Wu & Pollard 1992a). This phenomenon has been called 'saturation model' (Cobbold 1979), 'saturated with joints' (Narr 1991), and 'saturation level' (Narr & Suppe 1991) from field observation, as well as 'saturation of cracking' (Wu 1991), 'fracture saturation' (Wu & Pollard 1992a), and 'saturation level' (Rives *et al.* 1992) from experimental observation. We suggest using the term *fracture saturation*.

According to Cobbold (1979), 'the spatial interval between neighbouring structures (fractures in this case) has a limited range of values,' after saturation. The phenomenon was discussed by Narr & Suppe (1991) in reference to stages in the development of a joint set in the Monterey Formation of California. They envisioned that joint spacing was closely related to tectonic strain in the early stages, but later deformation was accommodated by opening the existing joints rather than creating new ones. Because the outcrop data gave nearly constant values of the fracture-spacing index (FSI ≈ 1.3), they described these strata as being saturated with joints. Rives *et al.* (1992) appeal to this same phenomenon and suggest that the final stage of development, that characterized by a normal distribution of spacing, corresponds to the saturation level. Furthermore they use the mode/mean ratio for spacing distribution as a measure of this saturation level.

Demonstration that a fracture set reaches saturation with respect to strain magnitude has important implications for the interpretation of field data. Measurements of spacing from two outcrops of the same rock unit with the same thickness and a poorly-developed joint set could be quite different because minor differences in strain would lead to major differences in spacing. This fact, along with the errors introduced by the line method of measurement, could explain the considerable scatter in some field data reported in the literature. Furthermore, plotting spacing vs thickness from poorly-developed joint sets in different rock units on the same graph is unlikely to lead to meaningful insights about the material properties of these units, because spacing is so sensitive to the applied strain. On the other hand, spacing data could provide a good constraint on strain magnitude for poorly-developed sets if the relationship between spacing and strain were known.

The implications of saturation for field data on a well-developed joint set are quite different. For example, one should not expect to be able to infer the strain magnitude from measurements of spacing on a well-developed joint set because a wide range of strains produce nearly the same spacing. On the other hand this same fact provides some justification for plotting spacing vs thickness for different rock units to understand possible differences in their material properties. Clearly one of the first items to consider when gathering spacing data is how well the joint set is developed.

Comparing the two extreme thicknesses from our experiments, $T = 0.016$ and 0.373 mm, saturation spacing increases systematically from 0.20 to 4.8 mm under the same applied strain. Curves for four different thicknesses were calculated by least square fitting (Guest 1961) and are shown in Fig. 12(h). The relationship between spacing and strain is a non-linear decreasing function which apparently approaches successively greater asymptotes of constant spacing for greater thicknesses. Development of similar curves from outcrop data would provide the basis for inferring strain states for rock units with poorly-developed joint sets.

Relationship between thickness and spacing at saturation

The relationship between layer thickness and fracture spacing at *fracture saturation* in the brittle coating is plotted in Fig. 13. Each point on this graph represents the mean value of several measurements of spacing S at a strain of 4.5×10^{-3}. Standard deviations for the spacing range from ±0.022 mm for $T = 0.016$ mm to ±0.890 mm for $T = 0.373$ mm as indicated by error bars. When applied strains are greater than 4.5×10^{-3}, fractures are essentially saturated (Fig. 13). Although there is considerable scatter in the data on spacing, particularly for the thick specimens, the slope of the curve in this figure is positive. The best fit straight line (dashed in Fig. 14) has a slope $S/T = 11.2$. On the other hand, least square fitting a curved line to the data gives a local slope $dS/dT = 9.1$ at $T = 0.1$ mm and $dS/dT = 11.7$ at $T = 0.3$ mm suggesting the relationship is not linear.

The relationship between S and T shown in Fig. 14 (solid curve) has the following form:

$$\frac{dS}{dT} > 0 \quad \text{and} \quad \frac{d^2S}{dT^2} > 0. \tag{8}$$

Spacing increases with thickness and has a positive curvature (concave upward).

The positive second derivative is not the relationship suggested by some field data and given in (1). As we mentioned before, the experiments reported here were conducted in just a few minutes, but in other experiments, where applied strains did not change with time for a few hours, we observed that spacing is time dependent. For example, under strain cycling, spacing depends on the details of the loading history (Wu & Pollard 1992a). Based on these experiments we suggest that more complex loading histories could provide explanations for the differences represented by some field data (1) and the experiments (8).

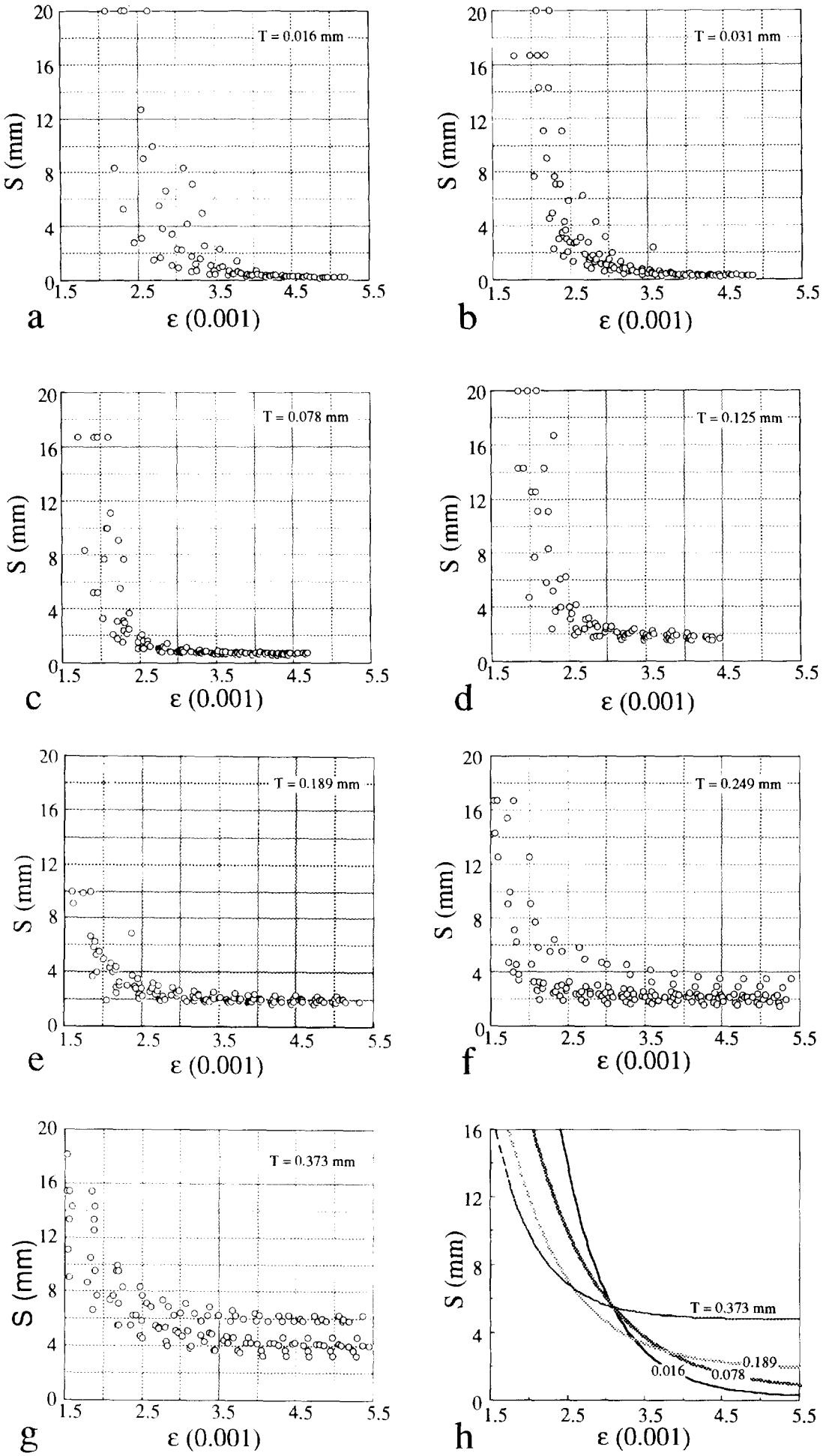
T = 0.016 mm
T = 0.031 mm
T = 0.078 mm
T = 0.125 mm
T = 0.189 mm
T = 0.249 mm
T = 0.373 mm
0.016
0.078
0.189
S (mm)
ε (0.001)
a
b
c
d
e
f
g
h

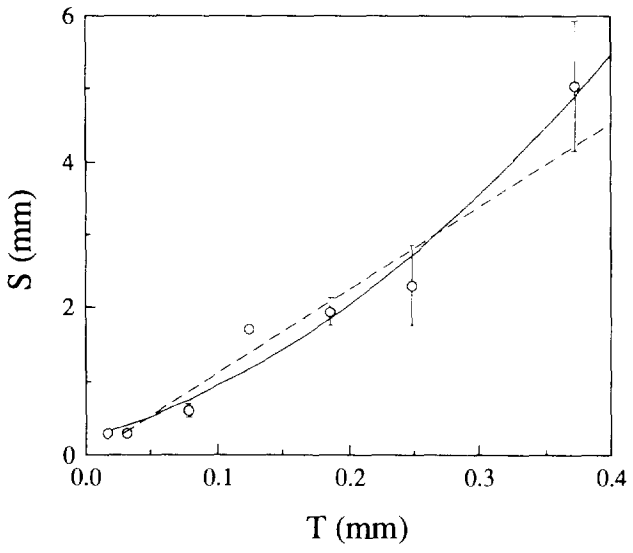

Fig. 13. Experimental results on the spacing–thickness relationship for a maximum applied strain of $\varepsilon_0 = 4.5 \times 10^{-3}$. The data are representative of the state of fracture saturation. The best fit straight line (dashed) and curve (solid) using least squares are shown for comparison.

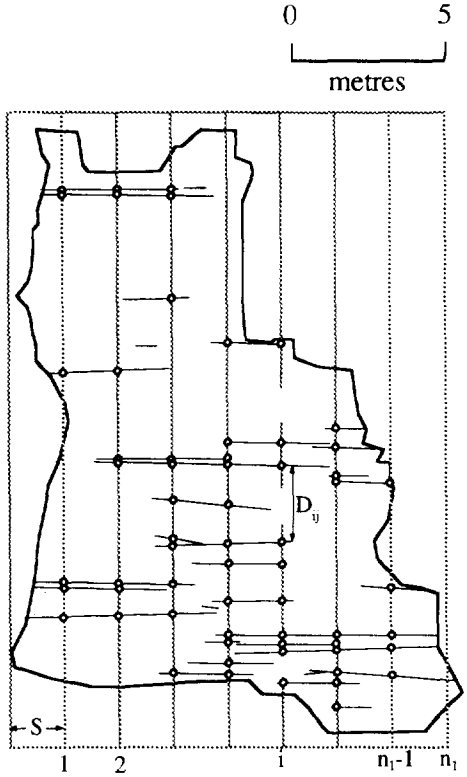

Fig. 14. Example of the estimation of the degree of fracture saturation, d, using equation (9) for the outcrop shown in Fig. 8. $n_1 = 7$, $n_2(i) = 5, 7, 10, 11, 9, 9, 4$ ($i = 1, \ldots, 7$), $d = 0.940$.

DEGREE OF FRACTURE SATURATION

To describe fracture saturation quantitatively, the deviation, d, of normalized individual spacings, D_{ij}, from the area spacing, S, is a good indicator. In general, a low deviation represents a high degree of fracture saturation. The deviation can be calculated as follows:

$$d = \sqrt{\frac{1}{\sum_{i=1}^{n_1} n_2(i)} \sum_{i=1}^{n_1} \sum_{j=1}^{n_2} \left(\frac{D_{ij}}{S} - 1 \right)^2}, \quad (9)$$

where n_1 is the number of scanlines along the direction perpendicular to fractures (Fig. 14), $n_{2(i)} + 1$ is the number of fractures intersected by scanline i, S is the spacing by the area method, and D_{ij} is the individual spacing between two neighboring fractures j and $j + 1$ on scanline i. Equation (9) can be used for joint systems exposed on bedding surfaces. It is suggested that the interval between two neighboring scanlines be S; apparently an even smaller interval and more scanlines provide a somewhat more accurate d. Figure 14 shows the field map from Dunne & North (1990) with an example calculation of deviation: there are a total of seven scanlines, 62 intersecting points, and 55 individual spacings. Inputting these data into equation (9), we find $d = 0.940$.

For wellbores or bedding cross-sections where S cannot be measured and individual spacings can be measured in only one scanline, d becomes

$$d = \sqrt{\frac{1}{n_2} \sum_{j=1}^{n_2} \left(\frac{D_j}{D} - 1 \right)^2}, \quad (10)$$

where n_2 is the number of joints intersected by the scanline, D_j is the individual spacing between two neighboring joints j and $j + 1$ on the scanline, and D is the mean value of D_j.

A qualitative classification of fracture (joint) sets related to the degree of fracture saturation is proposed based on ranges of the spacing deviation, d (Table 1). The degrees of fracture saturation for the two field examples shown in Figs. 8 and 9 were calculated using equation (9) and compared with Table 1. In the first example, d is 0.940, so the joint pattern is classified as poorly-developed. In the second example, d is 0.336, so the joint pattern is well-developed. Similarly, the first experimental example (Fig. 5a) with $d = 0.606$ is poorly- to intermediately-developed and the second experimental example (Fig. 5b) with $d = 0.450$ is intermediately- to well-developed.

CONFINED AND UNCONFINED BLOCKS

An important difference between natural joints in rock units and experimental fractures in brittle coating is

Fig. 12. Spacing vs applied strain for different thicknesses: (a) $T = 0.016$ mm, seven experiments; (b) 0.031 mm, nine experiments; (c) 0.078 mm, 10 experiments; (d) 0.125 mm, 10 experiments; (e) 0.189 mm, 10 experiments; (f) 0.249 mm, 11 experiments; (g) 0.373 mm, 10 experiments; and (h) least square fitting. Since spacing in a poorly-developed fracture set is very sensitive to the applied strain, curve fitting in (h) is not accurate for strains from 1.5×10^{-3} to 3.5×10^{-3}.

Table 1. Classification of fracture (joint) sets

Degree of saturation, d	Qualitative description of fracture (joint) pattern
>0.70	Poorly-developed
0.60 ~ 0.70	Poorly- to intermediately-developed
0.50 ~ 0.60	Intermediately-developed
0.40 ~ 0.50	Intermediately- to well-developed
<0.40	Well-developed

the very different top boundary conditions. A particular rock unit at depth in the earth is confined, and perhaps bonded, on its top and bottom surfaces to the adjacent rock units. On the other hand the brittle coating is bonded to the PMMA substrate and has a traction-free top surface. One possible manifestation of these different boundary conditions is a different ratio of spacing to thickness for well-developed fracture sets. For experiments reported here this ratio ranges from 9 to 12 whereas typical values for jointed rock range from 0.5 to 2.

We hypotheses that the larger ratio of spacing to thickness for the experimental fractures is caused, at least in part, by the traction free top surface and the lack of overburden (Fig. 10). In contrast, the smaller ratios for jointed rock are attributed, at least in part, to confinement by adjacent strata. To test this hypothesis we investigate the stress distributions in a two-dimensional numerical model (Fig. 15) using the boundary element method to solve this linear elastic problem (Crouch & Starfield 1983). This is not a model of joint propagation so we are justified in ignoring the three-dimensional aspects of that phenomenon. Rather we want to compare stress distributions between existing fractures in confined and unconfined blocks to see which is greater. Then we suggest that greater stress would be consistent with the formation of a fracture between the two existing fractures, thereby promoting a smaller spacing to thickness ratio.

Because of symmetry we can isolate a block bounded on the right-hand end by a vertical joint and on the left-hand end by the mid-plane between this joint and its neighbor. The loading of this block is related to the stretching of the composite material in the x-direction and the weight of the overlying material acting in the y-direction. Specifically, the boundary conditions include a sinusoidal distribution of tangential displacement on the bottom boundary of the unconfined block (Fig. 15a) and on both the top and bottom boundaries of the confined block (Fig. 15b). The imposed displacement distribution results in a cosinusoidal distribution of the strain ε_{xx}, thus providing a maximum strain at $x = 0$ and no strain at $x = H/2$, where H is the spacing between two joints. Overburden for the confined block was chosen to be representative of depths equal to 500 m. Poisson's ratio is 0.25, Young's modulus is 7000 MPa, and density is 2600 kg m^{-3}.

Based on the assumption that the two horizontal boundaries of the confined block should be flat before and after deformation, a vertical constant displacement is applied on the confined block (Fig. 15). The boundary conditions for the two blocks can be written as:

$$u_x = \frac{\varepsilon_0 H}{\pi} \sin\left(\frac{\pi x}{H}\right),$$
$$u_x = \pm u_{y0}\left(0 < x < \frac{H}{2},\ y = 0 \text{ and } T, \text{confined}\right), \tag{11}$$

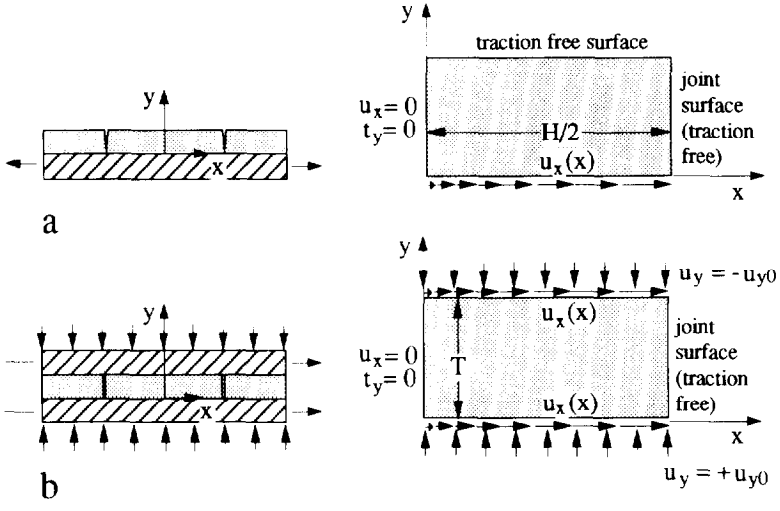

Fig. 15. Numerical models used to compare the state of stress for an unconfined block and a confined block. (a) Unconfined block with a traction free top surface. (b) Confined block with prescribed displacement boundary conditions. Applied maximum strain, $\varepsilon_0 = 3 \times 10^{-3}$, does not change in the x direction. Displacement u_{y0} depends on overburden depth.

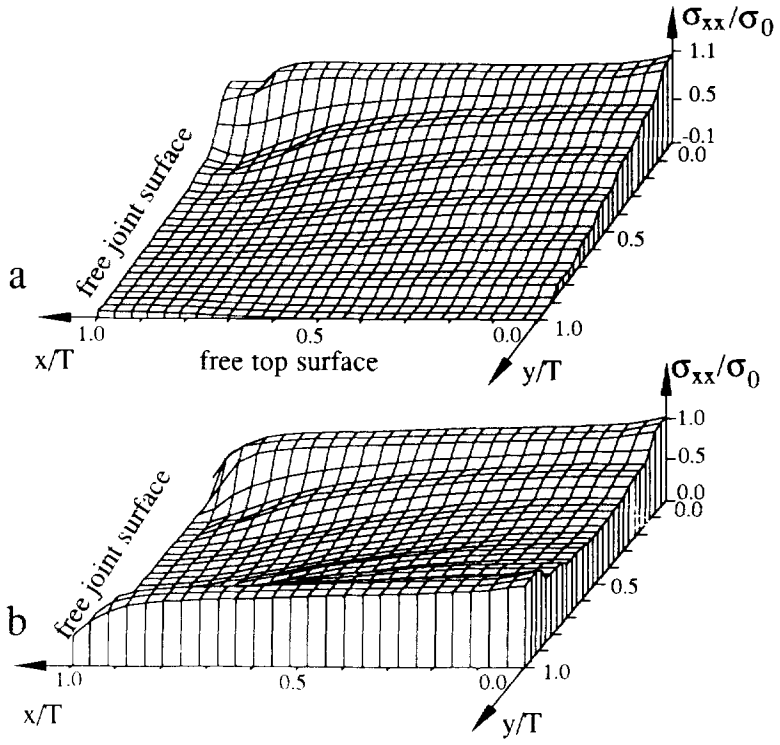

Fig. 16. The distribution of stress component σ_{xx} normalized by remote stress, σ_0 along x and y: (a) in the unconfined block; and (b) in the confined block. T is layer thickness; H is distance between joints; and $H/T = 2$.

$$t_x = t_y = 0 \left(0 < x < \frac{H}{2},\ y = T, \text{unconfined}\right), \tag{12}$$

$$u_x = \frac{\varepsilon_0 H}{\pi} \sin\left(\frac{\pi x}{H}\right),$$

$$u_y = 0 \left(0 < x < \frac{H}{2},\ y = 0, \text{unconfined}\right), \tag{13}$$

$$u_x = 0, \quad t_y = 0 \ (x = 0, 0 < y < T, \text{both}), \tag{14}$$

$$t_x = t_y = 0 \left(x = \frac{H}{2},\ 0 < y < T, \text{both}\right), \tag{15}$$

where $\varepsilon_0 (= 3 \times 10^{-3})$ is the applied strain in x direction, $u_{y0} (= 1.27 \times 10^{-3} T)$ is the magnitudes of displacements on the bottom and top boundaries associated with three different overburdens, t_x and t_y are traction components, and T is block thickness. The boundary conditions for the unconfined block are believed to be similar to those of the experimental models in which strain is transmitted from the PMMA substrate into the brittle coating except near the tiny interfacial regions around fractures.

The tensional normal stress, σ_{xx}, acting parallel to the layer, is normalized to the remote stress in x direction, σ_0, and plotted as a function of y/T at different locations x/T in Fig. 16. The stress component σ_{xx} provides the driving force for vertical fracture propagation. In the lower half of both blocks ($0 < y < T/2$) this stress component is on the order of the tensile strength of rock, and the stress in the unconfined block is similar to that in the confined block. However, in their upper halves ($y > H/2$) this stress component in the confined block is significantly greater than that in the unconfined block. The vertical component of normal stress, σ_{yy}, due to the overburden weight is 0 for the unconfined block and approximately -18 MPa for the confined block. This vertical stress would promote fracture propagation parallel to the y direction, much like the load in uniaxial compression tests promotes axial cracking (Singh 1970, Peng & Johnson 1972, Bombolakis 1973, Holzhausen 1977). These results suggest that fractures would propagate more easily through the confined block, and therefore the unconfined block would have a greater fracture spacing for the same thickness and the same extensional strain (Fig. 17).

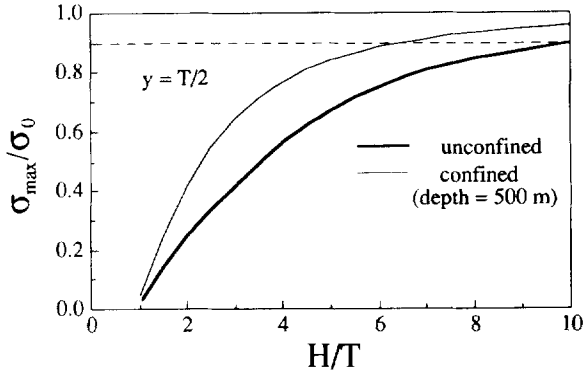

Fig. 17. Comparison of σ_{max}/σ_0 at $y = T/2$ in the unconfined and the confined blocks. $\sigma_{max} = \sigma_{xx}$ ($x = 0$, $y = T/2$). At the same stress level (dash line), spacing in the confined block is smaller than that in the unconfined block.

Our analysis does not explicitly address the contribution made to the joint spacing by differences in mechanical properties between layers. Gross *et al.* (in press) show the effect of mechanical property differences on the stress distribution in a fractured layer. This effect can be equivalent to different boundary conditions imposed on the blocks in our model. For instance, if the remote stress does not change, increasing the Young's moduli of the top and bottom layers will result in a decrease in the strain applied on the fractured layer.

CONCLUSIONS

Two methods for measuring fracture spacing have been described and compared. Spacing S measured by the *area method* has a single value for a given outcrop or experimental area and is not affected by fracture distribution within that area. In contrast, spacing D measured by the *line method* can depend on the location of the traverse across that area. S is a function of the size of the measurement area and the total length of fractures within that area. The area method requires measurement on layer surfaces, whereas the line method can be used either on cross-sections or surfaces.

Two kinds of fracture patterns are distinguished on bedding surfaces and in laboratory specimens. One, termed *poorly-developed*, is characteristic of the early stages in the development of a fracture set when typical fracture lengths are roughly equal to or less than typical spacings. The other, termed *well-developed*, is characteristic of the later stages when fracture lengths are much greater than spacings. The area method of spacing measurement is applicable to rock units with poorly-developed joint sets and with well-developed sets. In contrast, the line method fails to produce consistent results for poorly-developed joint sets.

The accuracy of spacing measurements depends on the size of the measured area. If the area is too small the sample will not be representative of the joint set; if the area is too big it may include real spatial variations in spacing. Roughly speaking, the characteristic dimension of the region, l_0, should be much greater than mean spacing, S. On the other hand, the size of the region should be small enough to lie within a single joint domain (Kulander & Dean 1980a,b, 1983, Isachsen *et al.* 1983, Wu & Cruikshank 1992, Cruikshank & Aydin in press).

In most mechanical anaylses of joint spacing in layered rocks two-dimensional fracture propagation is assumed to be perpendicular to bedding. However, surface textures on joint surfaces usually indicate that the dominant propagation direction is subparallel to bedding planes. The experimental models described in this paper produce fractures that propagate in the plane of the layer. Because of technical difficulties we currently are only able to experiment on a fractured layer with a traction-free top surface and a bottom surface that is bonded to a substrate. In contrast, natural joint sets form in layers that are confined both above and below. We suggest that key aspects of the evolution of fracture spacing in our laboratory models should be similar to those in a layer with top and bottom surfaces bonded to adjacent layers. However, all else being the same, our analysis suggests that the actual spacing in a doubly-bonded layer should be less than spacing in a layer with a free top surface.

An important concept that we have confirmed and quantified during these model experiments is *fracture saturation*, which is attributed to stress relaxation caused by fracture opening without significant fracture propagation. This concept has been discussed in the context of field observations (Cobbold 1979, Narr 1991, Narr & Suppe 1991) and experimental observations (Wu 1991, Rives *et al.* 1992, Wu & Pollard 1992a). As the applied strain increases the spacing decreases because existing fractures increase in length and new fractures begin to propagate from flaws. However, when the applied strain reaches a certain limiting value, the spacing stops evolving and remains nearly constant as the strain continues to increase. Our model experiments demonstrate that fracture spacing at saturation increases as a function of layer thickness, but spacing may not be linearly proportional to thickness. The deviation of normalized individual spacings, d, is a good indicator of fracture saturation. In general, a low d represents a high degree of fracture saturation.

DISCUSSION

Assessing the degrees of fracture saturation is a first-order consideration when gathering data to relate joint spacing and layer thickness. We encourage systematic field studies of the relationship between joint spacing and bed thickness that take the degree of saturation into account. We also encourage the measurement of spacing by the area method where that is practical.

Measurements of spacing from two outcrops in the same rock unit with the same thickness and a non-saturated joint set could be quite different because minor differences in strain produce major differences in spacing. Thus, plotting spacing vs thickness from poorly-developed joint sets in different rock units is unlikely to lead to meaningful insights about the material properties of these units. The implications for field data on a well-developed joint set are quite different. For example, one should not expect to be able to infer the strain magnitude from measurements of spacing on a well-developed joint set because a wide range of strains produce nearly the same spacing. On the other hand, this same fact provides justification for plotting spacing vs thickness for different rock units that are saturated with joints to understand possible differences in their material properties.

The concepts discussed above may be useful in the evaluation of joints using borehole data from a subsurface layer. Subsurface data on bed thickness have been readily obtained by standard logging techniques for many years (Schlumber 1989). However, nearly vertical boreholes in subhorizontal strata encounter few vertical

joints and provide a poor sampling of joint spacing within one bed. With the recent advent of inclined and horizontal drilling (Artindale *et al.* 1991, Fritz *et al.* 1991, Davenport 1992), and improved logging techniques (Schlumberger 1989) such as Borehole Televiewers (CBIL), Formation Micro Scanners (FMS or FMI), and Dipmeter measurements (FIL) as well as core samples, difficulties in the measurement of subsurface joint spacing can be overcome. Such spacing data may have to be corrected for the relative orientation of the borehole and the joint set (Narr 1991) and are, at best, typical of data taken using the line method. Therefore it is particularly important to assess the degree of fracture saturation. The processed borehole data can be used to rebuild subsurface joint networks, estimate joint connectivity, and predict drainage area around a borehole, taking advantage of the knowledge gained about the jointing process from fracture experiments (Wu *et al.* in press).

Given reliable borehole measurements of thickness and spacing, one needs a methodology for extrapolating this geometric data from the borehole into the surrounding formations. Joint spacing typically is viewed as the dependent variable (to be estimated) whereas bed thickness is the independent variable (fixed by the borehole measurement). By combining reliable subsurface data on joint spacing and bed thickness with a mechanical model for the process of joint formation one should be able to formulate a methodology for this extrapolation. If successful, this would have a profound effect on our understanding of fluid flow in fractured rock masses, and would provide valuable input parameters for reservoir and acquifer simulation models.

Acknowledgements—This research is supported by the U.S. Department of Energy under the grant DE-FG03-89ER14081-A001 and the Stanford Rock Fracture Project, Stanford University. The field trip to the coastal region at Gaviota, California was supported by a 1993 GSA research grant. The authors wish to thank Atilla Aydin and Kenneth M. Cruikshank, William M. Dunne and Colin P. North for their maps, and Michael R. Gross, two JSG reviewers, Tim Bevan and Thierry Rives for their helpful comments and review of this work.

REFERENCES

Angelier, J., Souffaché, B., Barrier, E., Bergerat, F., Bouaziz, S., Bouroz, C., Creuzot, G., Ouali, J. & Tricart, P. 1989. Distribution de joints de tension dans un banc rocheux: lio théorique et espacements. *C. r. Acad. Sci. Paris, Sér.* **II 309**, 2119–2125.

Artindale, J., Runions, G. A. & Smith, D. G. 1991. *Horizontal Wellbores: Geological Applications, Drilling and Completion Technology and Selection Criteria*. Canadian Hunter Exploration Ltd., Calgary, Alberta.

Bahat, D. 1991. *Tectono-fractography*. Springer-Verlag, Berlin.

Barton, C. C. & Larsen, E. 1985. Fractal geometry of two-dimensional fracture networks at Yucca Mountain, southwestern Nevada. *Proc. of Fundamentals of Rock Joints: Proc. of the International Symposium on Fundamentals of Rock Joints*. Björkliden, Sweden, 77–84.

Bear, J., Tsang, C.-F. & de Marsily, G. 1993. *Flow and Contaminant Transport in Fractured Rock*. Academic Press, San Diego, California, U.S.A.

Beyer, W. H. 1991. *Standard Mathematical Tables and Formulae*. CRC Press, Boca Raton, Florida, U.S.A.

Bogdanov, A. A. 1947. The intensity of cleavage as related to the thickness of beds. *Soviet Geol.* **16**.

Bombolakis, E. G. 1973. Study of the brittle fracture process under uniaxial compression. *Tectonophysics* **18**, 231–248.

Cacas, M. C., Ledoux, E., de Marsily, G., Barbreau, A., Calmels, P., Gaillard, B. & Magritta, R. 1990. Modeling fracture flow with a stochastic discrete fracture network; calibration and validation; 2, The transport model. *Water Resour. Res.* **26**, 491–500.

Cobbold, P. R. 1979. Origin of periodicity: saturation or propagation? *J. Struct. Geol.* **1**, 96.

Crouch, S. L. & Starfield, A. M. 1983. *Boundary Element Methods in Solid Mechanics*. George Allen and Unwin, London.

Cruikshank, K. M. & Aydin, A. In press. Fracture patterns in Entrada sandstone, southwest limb of Salt Valley anticline, Arches National Park, Utah, U.S.A. *J. Struct. Geol.*

Davenport, B. 1992. *Horizontal and Vertical Drilling*. McGraw-Hill, New York.

DeGraff, J. M. & Aydin, A. 1987. Surface morphology of columnar joints and its significance to mechanics and direction of joint growth. *Bull geol. Soc. Am.* **99**, 605–617.

Deloule, E. & Turcotte, D. L. 1989. The flow of hot brines in cracks and the formation of ore deposits. *Econ. Geol.* **84**, 2217–2225.

Dunne, W. M. & North, C. P. 1990. Orthogonal fracture systems at the limits of thrusting: an example from southwestern Wales. *J. Struct. Geol.* **12**, 207–215.

Engelder, T. 1987. *Joints and Shear Fractures in Rock*. Academic Press, London.

Fritz, R. D., Horn, M. K. & Joshi, S. D. 1991. *Geological Aspects of Horizontal Drilling*. Am. Assoc. Petr. Geol., Tulsa, Okla.

Garrett, K. W. & Bailey, J. E. 1977a. Multiple transverse fracture in 90° cross-ply laminates of a glass fibre-reinforced polyster. *J. Mater Sci.* **12**, 157–168.

Garrett, K. W. & Bailey, J. E. 1977b. The effect of resin failure strain on the tensile properties of glass fibre-reinforced polyster cross-ply laminates. *J. Mater Sci.* **12**, 2189–2194.

Gross, M. R. 1993. The origin and spacing of cross joints: examples from the Monterey Formation, Santa Barbara coastline, California. *J. Struct. Geol.* **15**, 737–751.

Gross, M. R., Fisher, M. P., Engelder, T. & Greenfield, R. J. In press. Factors controlling joint spacing in interbedded sedimentary rocks: Integrating numerical models with field observations. *Geol. Soc. Lond.*

Guest, P. G. 1961. *Numerical Methods of Curve Fitting*. Cambridge University Press, Cambridge.

Hancock, P. L. 1985. Brittle microtectonics: principles and practice. *J. Struct. Geol.* **7**, 437–457.

Helgeson, D. E. & Aydin, A. 1991. Characteristics of joint propagation across layer interfacies in sedimentary rock. *J. Struct. Geol.* **13**, 897–911.

Hobbs, D. W. 1967. The formation of tension joints in sedimentary rocks: an explanation. *Geol. Mag.* **104**, 550–556.

Hodgson, R. A. 1961. Classification of structures on joint surfaces. *Am. J. Sci.* **259**, 439–502.

Holzhausen, G. 1977. Axial and subaxial fracturing of Chelmsford Granite in uniaxial compression. In: *Energy Resources and Excavation Technology, Proc. 18th U.S. Symp. Rock Mech.* (edited by Wang, F. D. & Clark, G. B.). Colo. Sch. Mines Press, Golden, Colo., U.S.A., 3B7.1–3B7.7.

Huang, Q. & Angelier, J. 1989. Fracture spacing and its relation to bed thickness. *Geol. Mag.* **126**, 355–362.

Isachsen, Y. W., Geraghty, E. P. & Wiener, R. W. 1983. Fracture domains associated with a neotectonic, basement-cored dome; the Adirondack Mountains, New York. *Proc. 4th Int. Conf. Basement Tectonics* **4**, 287–305.

Kirillova, I. V. 1949. Some problems of the mechanics of folding. *Trans. Geofian* **6**.

Kulander, B. R., Barton, C. C. & Dean, S. L. 1979. Application of fractography to core and outcrop fracture investigation. Paper METC/SP-79/3, Washington, D.C., U.S.A. Government Printing Office, U.S. Department of Energy.

Kulander, B. R. & Dean, S. L. 1980a. Rome Trough relationship to fracture domains, regional stress history and decollement structures. In: *Proc. Symp. on Western Limits of Detachment and Related Structures in the Appalachian Foreland* (edited by Wheeler, R. L. & Dean, C. S.). 64–81.

Kulander, B. R. & Dean, S. L. 1980b. Basement structure relationship to stress history, fracture domains and décollement tectonics in southern West Virginia. In: *Circular—West Virginia Geol. and Economic Survey* **C-16**, 10.

Kulander, B. R. & Dean, S. L. 1983. Fracture domains in the Allegheny Plateau of West Virginia, In: *Circular—West Virginia Geol. & Economic Survey* **C-31**, 34–38.

Lachenbruch, A. H. 1961. Depth and spacing of tension cracks. *J. geophys. Res.* **66**, 4273–4292.
Ladeira, F. L. & Price, N. J. 1981. Relationship between fracture spacing and bed thickness. *J. Struct. Geol.* **3**, 179–183.
Lorenz, J. C., Teufel, L. W. & Warpinski, N. R. 1991. Regional fractures I: a mechanism for the formation of regional fractures at depth in flat-lying reservoirs. *Bull. Am. Ass. Petrol. Geol.* **75**, 1714–1737.
Mastella, L. 1972. Interdependence of joint density and the thickness of layers in the Podhale Flysch. *Bull. de l'Anlac. Pol. des sci.* **20**, 187–196.
McQuillan, H. 1973. Small-scale fracture density in Asmari formation of Southwest Iran and its relation to bed thickness and structural setting. *Bull. Am. Ass. Petrol. Geol.* **57**, 2367–2385.
Mihashi, H., Tokahashi, H. & Wittmann, F. H. (Eds) 1989. *Fracture Toughness and Fracture Energy: Test Methods for Concrete and Rock*. A. A. Balkema, Rotterdam.
Narr, W. 1991. Fracture density in the deep subsurface: Techniques with application to Point Arguello oil field. *Bull. Am. Ass. Petrol. Geol.* **75**, 1300–1323.
Narr, W. & Lerche, I. 1984. A method for estimating subsurface fracture density in core. *Bull. Am. Ass. Petrol. Geol.* **66**, 637–648.
Narr, W. & Suppe, J. 1991. Joint spacing in sedimentary rocks. *J. Struct. Geol.* **13**, 1037–1048.
Nelson, R. A. 1985. *Geologic Analysis of Naturally Fractured Reservoirs*. Gulf Publishing Co., Houston, Texas.
Norris, D. K. 1966. The mesoscopic fabric of rock masses about some Canadian coal mines. *Proc. Congr. Int. Soc. Rock Mech.* Lisbon, Portugal, **1**, 191–198.
Novikova, A. C. 1947. The intensity of cleavage as related to the thickness of the bed. *Soviet Geol.* **16**.
Peng, S. & Johnson, A. M. 1972. Crack growth and faulting in cylindrical specimens of Chelmsford Granite. *Int. J. Rock Mech. & Mining Sci. Geomech. Abstr.* **9**, 37–86.
Pollard, D. D. & Aydin, A. 1988. Progress in understanding jointing over the past century. *Bull. geol. Soc. Am.* **100**, 1181–1204.
Pollard, D. D. & Segall, P. 1987. Theoretical displacements and stresses near fractures in rock, with applications of faults, joints, veins, dikes, and solutionsurfaces. In: *Fracture Mechanics of Rock* (edited by Atkinson, B. K.). Academic Press, London, 277–349.
Pollard, D. D., Zeller, S., Wu, H. & Thomas, A. 1990. Origins of joint spacing distributions in sedimentary rocks: new results from numerical and physical model studies. *Geol. Soc. Am. Abstr.* **22**, 142.
Price, N. J. 1966. *Fault and Joint Development in Brittle and Semi-Brittle Rock*. Pergamon Press, Oxford.
Price, N. J. & Cosgrove, J. W. 1990. *Analysis of Geological Structure*. Cambridge University Press, Cambridge.
Rives, T. & Petit, J. P. 1990a. Jointing and folding: an experimental approach. *C. r. Acad. Sci. Paris* **310**, 1115–1121.
Rives T. & Petit, J. P. 1990b. Experimental study of jointing during cylindrical and noncylindrical folding. In: *Mechanics of Jointed and Faulted Rock*, (edited by Rossmanith, H. P.). Balkema, Rotterdam, 205–211.
Rives, T., Razack, M., Petit, J.-P. & Rawnsley, K. D. 1992. Joint spacing: analogue and numerical simulations. *J. Struct. Geol.* **14**, 925–937.
Rossmanith, H. P. (Ed.) 1983. *Rock Fracture Mechanics*. Springer-Verlag, New York.
Schlumberger, 1989. *Log Interpretation Principles/Applications*. Schlumberger Educational Services, Houston, Texas.
Singh, D. P. 1970. Mode of rock fracture in uniaxial compression. *Metals and Minerals Rev.* **9**, 3–6.
Souffaché, B. & Angelier, J. 1989. Distribution de joints de tension dans un banc rocheux: principle d'une modélisation énergétique. *Cr. r. Acad. Sci. Paris, Sér. II* **308**, 1385–1390.
Sowers, G. M. 1973. Theory of spacing of extension fracture. *Eng. Geol. Case Hist.* **9**, 27–53.
Syme-Gash, P. J. 1971. A study of surface features relating to brittle and semibrittle fracture. *Tectonophysics*. **12**, 349–391.
Thunvik, R. & Braester, C. 1990. Gas migration in discrete fracture networks. *Water Resour. Res.* **26**, 2425–2434.
Timoshenko, S. & Woinowsky-Krieger, S. 1959. *Theory of Plates and Shells*. McGraw-Hill Book Company, New York.
Underwood, E. E. 1972. The mathematical foundations of quantitative stereology. In: *Stereology and Quantitative Metallography*. Addison-Wesley, Reading, Massachusetts, 3–38.
Woodworth, J. B. 1896. On the fracture system of joints, with remarks on certain great fractures. *Boston Society of Natural Historical Proceedings*, **27**, 164–183.
Wu, H. 1991. Fracture sets in a brittle layer under uniaxial strain cycling. *Rock Fracture Project* Stanford University, **II**, B1–B7.
Wu, H. & Cruikshank, K. M. 1992. Formation of multiple fracture sets. *EOS, Tran.* **73**, 566.
Wu, H. 1992. Experimental simulation of the formation of multiple joint domains. *Rock Fracture Project* Stanford University, **III**, D1–D7.
Wu, H. & Pollard, D. D. 1991. Fracture spacing, density, and distribution in layered rock masses: results from a new experimental technique. In: *Rock Mechanics as a Multidisciplinary Science, Proc. 32nd U.S. Symp. Rock Mech.* (edited by Toegiers, J.-C.). Balkema, Rotterdam, 1175–1184.
Wu, H. & Pollard, D. D. 1992a. Propagation of a set of opening-mode fractures in layered brittle materials under uniaxial strain cycling. *J. geophys. Res.* **97**, 3381–3396.
Wu, H. & Pollard, D. D. 1992b. Modeling a fracture set in a layered brittle material. *Eng. Frac. Mech.* **42**, 1011–1017.
Wu, H., Willemse, E. J. M. & Pollard, D. D. In press. Prediction of fracture density and connectivity in layered rock masses using borehole data. In: *Proc. Eurock'94: Rock Mechanics in Petroleum Engineering*. Delft, the Netherlands.
Zeller, S. S. & Pollard, D. D. 1992. Boundary conditions for rock fracture analysis using the boundary element method. *J. geophys. Res.* **97**, 1991–1997.

APPENDIX A

Two special cases for the area method

Area method for regular and irregular polygons. Assume that there are m points along the periphery with coordinates (x_k, y_k) $(k = 1, 2, \ldots, m)$ and a reference point (x_0, y_0) within the polygon. Then m small triangles are formed by connecting those points (Fig. A1a) and the sides of these triangles have the lengths:

$$a_k = \sqrt{(x_{k+1} - x_k)^2 + (y_{k+1} - y_k)^2}, \quad \text{(A1)}$$

$$b_k = \sqrt{(x_k - x_0)^2 + (y_k - y_0)^2}. \quad \text{(A2)}$$

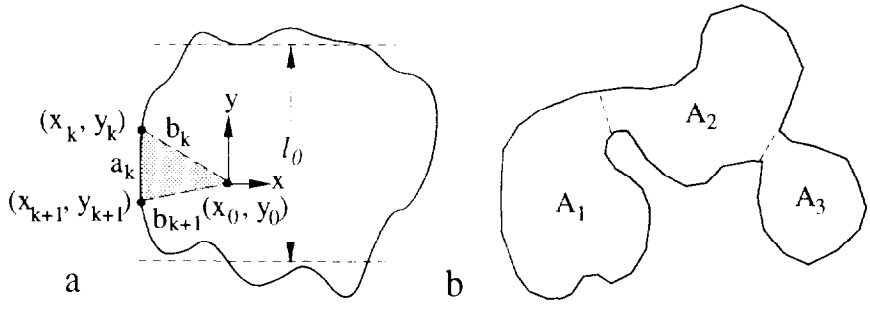

Fig. A1. Two special cases for the area method: (a) the area of a regular polygon is approximated by the areas of a series of small triangles, and (b) an irregular polygon may be decomposed into regular polygons.

The polygon area is expressed using Heron's formula for each triangular region and then summing (Beyer 1991):

$$A = \sum_{k=1}^{m} \sqrt{c_k(c_k - a_k)(c_k - b_k)(c_k - b_{k+1})}, \quad \text{(A3)}$$

$$c_k = \frac{a_k + b_k + b_{k+1}}{2} \quad (b_{m+1} = b_1). \quad \text{(A4)}$$

Substituting (A3) and (A4) into (3), the mean spacing for a regular polygonal area can be obtained:

$$S = \frac{\sum_{k=1}^{m}\sqrt{(a_k+b_k+b_{k+1})(a_k-b_k+b_{k+1})(a_k+b_k-b_{k+1})(-a_k+b_k+b_{k+1})}}{4\left(l_0 + \sum_{i=1}^{n} l_i\right)}$$

$$= \frac{A}{l_0 + L}. \quad \text{(A5)}$$

Here A is the area of the polygonal region and l_0 is the mean length of the region parallel to the fractures.

An irregular polygon can be divided into several regular polygons. For example, if there are three subregions (Fig. A1b) and they have similar fracture density, the weighted average spacing for the whole region is:

$$S = S_1w_1 + S_2w_2 + S_3w_3, \quad \text{(A6)}$$

$$A = A_1 + A_2 + A_3, \quad \text{(A7)}$$

where S_i is the spacing of subregion i and $w_i = L_i/L$ is the weight. If the total fracture length for each subregion, L_i, is much greater than the mean length, l_{0i}, equation (A6) can re rearranged and simplified:

$$S = \frac{A_1}{l_{01} + L_1}\frac{L_1}{L} + \frac{A_2}{l_{02} + L_2}\frac{L_2}{L} + \frac{A_3}{l_{03} + L_3}\frac{L_3}{L} \approx \frac{A}{L}. \quad \text{(A8)}$$

This is similar to (3) if l_0 is negligible compared to L. Equation (3) is applicable to square, regular and irregular polygons. To calculate mean spacing, we only need to know the area of the outcrop or laboratory specimen and the total length of fractures inside the area.

Area method for a well-developed fracture pattern. For a well-developed fracture pattern each individual spacing D_i is composed of the mean spacing D and a difference ΔD_i:

$$D_i = D + \Delta D_i. \quad \text{(A9)}$$

By multiplying l_i by D_i the polygon area is approximately estimated as follows

$$A = \sum_{i=0}^{n} l_iD_i \approx Dl_0 + DL + \sum_{i=1}^{n} l_i\Delta D_i. \quad \text{(A10)}$$

Since $L \gg l_i$, ΔD_i is either positive or negative and $\sum_{i=0}^{n} \Delta D_i = 0$, the last term of (A10) on the right-hand side is negligible. Rearrange (A10)

$$D \approx \frac{A}{l_0 + L} = S. \quad \text{(A11)}$$

Thus equations (3) and (4) are applicable for a well-developed fracture pattern within a polygon.